



Experimental study on the failure characteristic and mechanism of granite time-delayed rockburst under true triaxial condition

Guang-liang Feng · Qi Ma · Giuseppe Lacidogna · Peng-zhi Pan · Zhao-feng Wang · Guo-shao Su

Received: 7 September 2023 / Accepted: 29 November 2023
© The Author(s) 2023

Abstract A series of tests for time-delayed rockburst of granite under true triaxial condition was designed and carried out. By using the true triaxial rockburst test system, an acoustic emission (AE) system, a high-speed camera system, and a digital image motion analysis software, the time-delayed rockburst development process was monitored and studied. Four stages were found in the failure of granite time-delayed rockburst, i.e. grains ejection, slab breaks and ejects, first fragments ejection and second fragments

ejection. There is a “V” shear crack generated in the time-delayed rockburst sample, and several tensile cracks in the lower part of the rock sample cross through the “V” shear crack. The longer the duration (the time elapsed between the moments the AE hits rises rapidly and the rockburst occurs), the smaller the depth of the rockburst pit. The time-delayed rockburst debris are mainly composed of blocks and fragments. The longer the duration, the smaller the total debris mass, the percentage of ejected debris and the ejection kinetic energy. The fractal dimension of the debris is positively correlated with the duration. The longer the duration, the higher the degree of fragmentation. The cracks generated are tensile-shear composite cracks. In the loading stage, it is dominated by shear cracks. However, in the time-lag stage, it is dominated by tensile cracks. With the increase of the duration, the proportion of tensile cracks increased and the proportion of shear cracks decreased. The research results will have a certain reference value for the warning and risk mitigation of time-delayed rockbursts.

G. Feng (✉) · Q. Ma · P. Pan · Z. Wang
State Key Laboratory of Geomechanics and Geotechnical Engineering, Institute of Rock and Soil Mechanics, Chinese Academy of Sciences, Wuhan 430071, Hubei, China
e-mail: glfeng@whrsm.ac.cn

G. Feng · G. Su
Guangxi Key Laboratory of Disaster Prevention and Engineering Safety, Nanning 530004, Guangxi, China

G. Feng
Hubei Key Laboratory of Disaster Prevention and Mitigation, China Three Gorges University, Yichang 443002, Hubei, China

Q. Ma
University of Chinese Academy of Sciences, 100049 Beijing, China

G. Lacidogna
Department of Structural, Geotechnical and Building Engineering, Politecnico di Torino, Corso Duca DegliAbruzzi 24, 10129 Turin, Italy

Highlights

- Four stages were found in the failure of granite time-delayed rockburst.
- The longer the duration, the smaller the total debris mass, the percentage of ejected debris and the ejection kinetic energy.

- The loading stage is mainly resembled with shear cracks, while the time-lag stage is mainly with tensile cracks in the time-delayed rockburst.

Keywords True triaxial · Time-delayed rockburst · Crack evolution characteristics · Macro failure characteristics · AE

1 Introduction

With the rapid development of the world economy, the demand for underground resources has been increasing. A large number of underground projects with a large burial depth are planned, are under construction, or have been built. The burial depth and the in-situ stress level are increasing, and the geological environment of rock mass is becoming complex. Therefore, subsequent geological disasters are more frequent (Wu et al. 2019; Bai et al. 2021; Wang et al. 2016; Guo et al. 2023; Bai et al. 2019). A rockburst is defined as damage to an excavation that occurs in a sudden or violent manner and is associated with a seismic event (Hedley 1992; Kaiser et al. 1996). Rockbursts are characterized by being highly sudden, random and hazardous (Feng et al. 2019, 2015a, 2015b). In recent years, rockbursts occurred in a number of underground projects. For example, on November 28, 2009, an extremely intense rockburst occurred in a drainage tunnel of the Jinping II hydropower station in China, resulting in destruction of construction vehicles, seriously affecting the construction progress (Chen et al. 2012). On May 31, 2015, an extremely intense rockburst occurred in the deep tunnel of the Neelum-Jhelum hydropower project in Pakistan, which seriously affects the project (Feng et al. 2019; Feng et al. 2023, 2023b). There are rockbursts in Shizuizi copper mine, Pangushan tungsten mine and Gongchangling iron mine (Jiang et al. 2019). Many projects in Japan, Norway, and Sweden have experienced rockbursts to various degrees (Ortlepp 2005; Rudajev 1993). These rockbursts seriously threaten the safety of people's lives and property, greatly affect the safety construction of underground projects, and also bring unprecedented challenges to engineering design and construction.

According to the time characteristic of the rockbursts, the types of rockbursts can be divided into

immediate rockburst, time-delayed rockburst and intermittent rockburst (Feng et al. 2019). Time-delayed rockbursts are characterized by the occurrence of a period of time after excavation and unloading. For example, in the 2# diversion tunnel of Jinping II hydropower station, a time-delayed rockburst occurred 58 days after excavation (Chen et al. 2012). There were also many time-delayed rockbursts in Taipingyi hydropower station diversion tunnel, Tianshengqiao II hydropower station diversion tunnel, Ertan hydropower station diversion tunnel, etc.

A large number of scholars have carried out a series of studies on time-delayed rockbursts through on-site monitoring, indoor experiments, numerical simulations, theoretical analysis and other means. For example, Chen et al. (2012) carried out a systematic study of the time-delayed rockburst in the deep tunnels of Jinping II hydropower station. Based on field cases and monitoring data analysis, the temporal and spatial characteristics of the time-delayed rockburst and its evolution law and mechanism were revealed. He et al. (2010, 2012) carried out the true triaxial unloading rockburst test based on the self-developed true triaxial testing machine. The mechanism of time-delayed rockburst was preliminarily discussed. Chen et al. (2020) conducted the uniaxial compression with acoustic emission, elastic wave velocity and SEM scanning test, and explored the mechanism and precursory characteristics of time-delayed failure of granite in Southwest China. Fan et al. (2015) analyzed the energy dissipation during the cracking of surrounding rock masses, and revealed the difference in the evolution characteristics of time-delayed and immediate rockbursts under blasting and TBM (Tunnel Boring Machine) methods. Zhang et al. (2020) summarized the characteristics of delayed rockbursts and analyzed its formation process.

The immediate rockbursts have been studied for a long time (Feng et al. 2019, 2016; Su et al. 2016). However, for the time-delayed rockbursts, the related studies are limited, and the failure mechanics and characteristics need further study. In deep engineering, the rockmass is in a true triaxial stress state. The stress state of the surrounding rock changes due to the influence of excavation unloading. Compared with uniaxial and conventional triaxial tests, true triaxial test with five sides loading & one side free can better simulate the actual stress state of the surrounding rockmass with free face after excavation. However,

the experimental study of time-delayed rockburst under true triaxial test with five sides loading and one side free has rarely been reported, and the failure characteristics and internal crack evolution characteristics under corresponding condition are unclear.

In this paper, the granite time-delayed rockburst test under true triaxial condition with AE monitoring and high-speed camera system was designed and carried out. The rock sample is in a stress state with five sides loading and one side free. The maximum principal stress was designed by the AE hits. To some extent, this procedure simulates the time-delayed rockburst process in the actual excavation course. The stress and strain characteristics, eruption process, macro failure pattern and debris characteristics of granite time-delayed rockburst sample under the free face true triaxial condition were analyzed. Combined with the AE monitored data, the eruption process of granite time-delayed rockburst was analyzed and its internal crack evolution characteristic was revealed.

2 Experimental methodology

2.1 Test equipment

The test equipment is mainly composed of a true triaxial test loading system, an deformation sensing measurement system, an AE system, and a high-speed camera system (Fig. 1). The testing machine adopts a full digital servo controller to run the loading and unloading phases. By using the rigid loading pusher in the X, Y, Z directions, it can make three perpendicular independent loading and unloading.

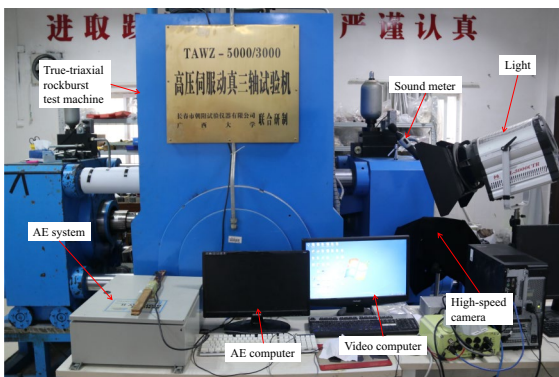


Fig. 1 True triaxial rockburst test system

The maximum loading capacity is 5000 kN vertically, and the maximum loading capacity is 3000 kN in the horizontal direction. The testing machine is equipped with a single-sided pendulum unloading device, which can quickly form the stress path from a six-sides loading to a five-sides loading and a side free, so as to simulate the stress state of surrounding rock during underground engineering excavation. The high-speed camera system includes SVSI GigaView high-speed cameras which can observe the ejection failure process. By using the professional digital image motion analysis software Image ProPlus 7.0, the flight trajectory of the ejection fragment on the free face can be captured. Then the total kinetic energy of the ejection fragment can be calculated based on the flight distance and its time. The high-speed camera system layout is shown in Fig. 2 (Su et al. 2016).

2.2 Engineering background and rock samples

The rock samples were from a deep engineering in western China. The maximum buried depth of the project is 2080 m and the measured local stress is ~45 MPa. Time-delayed rockbursts occurred during the construction of the project. Due to the sudden and violent nature of time-delay rockburst, it seriously endangers construction safety. A piece of host rock in the deep section of the project was collected to make rock samples with dimensions of 100 mm×100 mm×200 mm. And they were used to carry out true triaxial time-delayed rockburst test research. The density of the rock sample is 2632.5 kg/m³ and the average uniaxial stress is 160.2 MPa. The integrity and uniformity of the rock samples are good. The mineral composition of the rock samples was analyzed, and the main components were feldspar, quartz, chlorite, mica and carbonate minerals, with the proportions of 41%, 44%, 10% and 5%, respectively. Among them, the feldspar particle size is about 1.5 mm and the quartz particle size is about 3 mm. One rock sample is shown in Fig. 3.

2.3 Test scheme

After the project is excavated, the tangential stress of the surrounding rock will change and concentrate, and after a period of time, it will remain stable. After that, if a rockburst occurs, it belongs to time-delayed

Fig. 2 Layout of high speed camera system (Su et al. 2016)

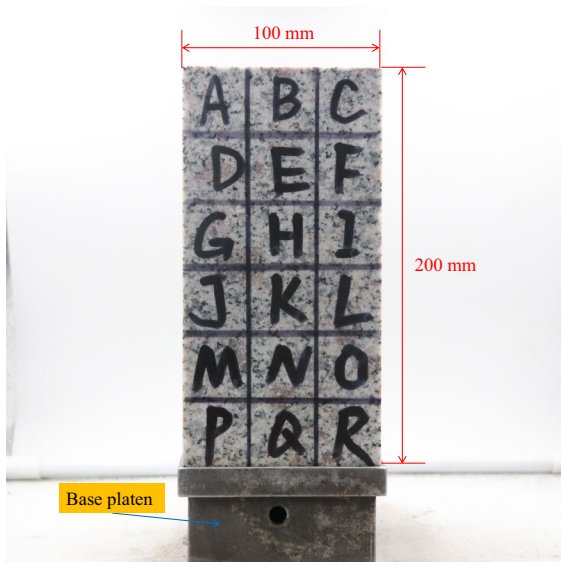
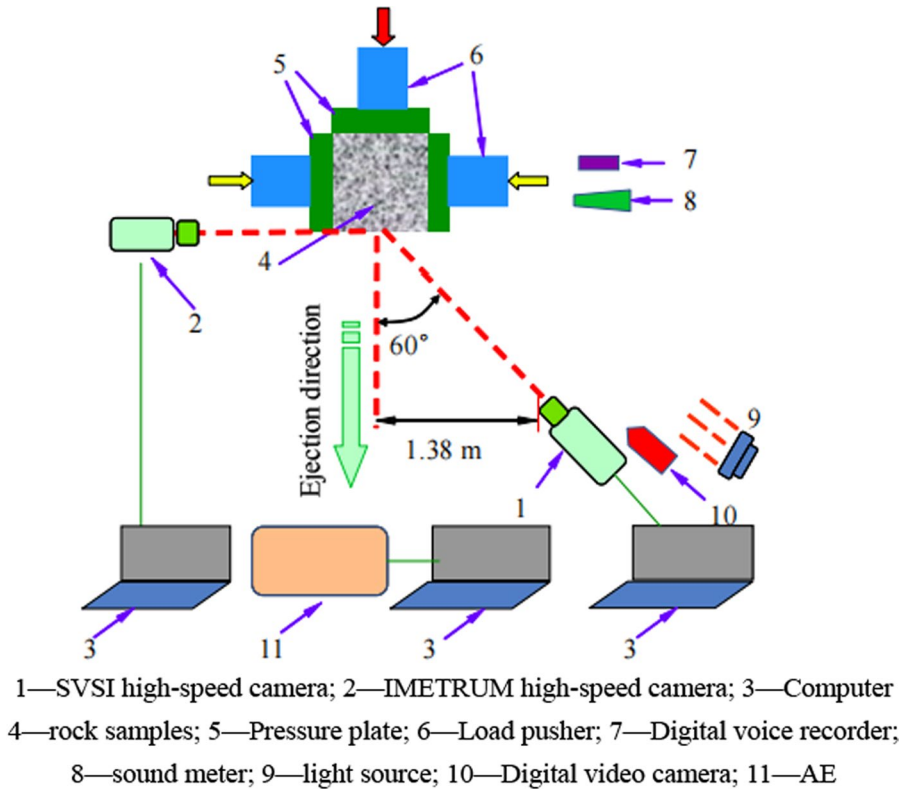
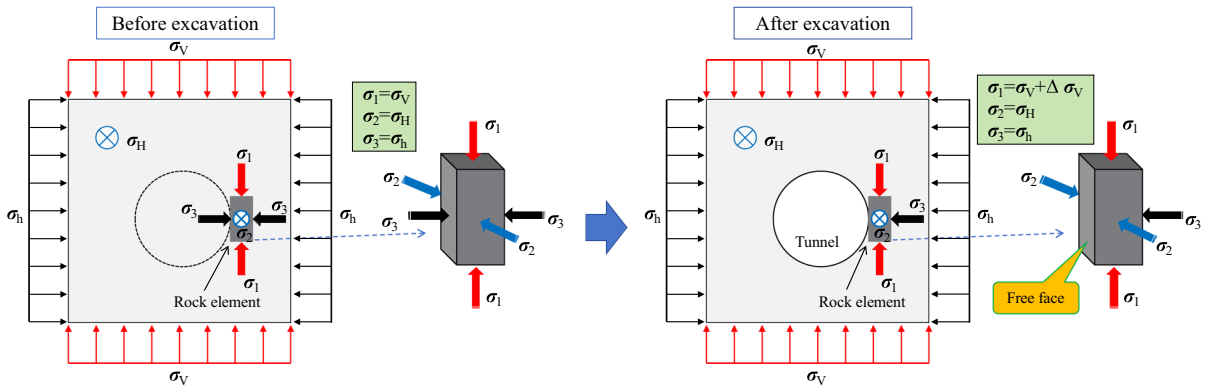


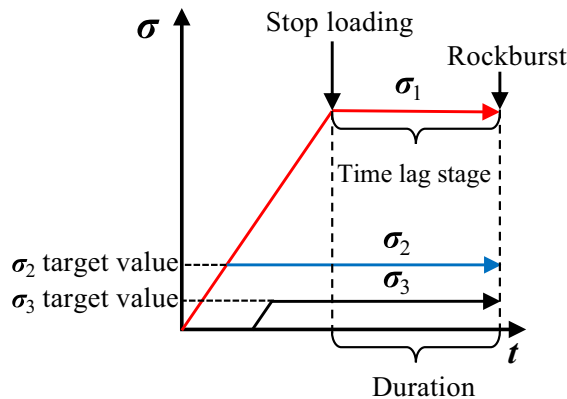
Fig. 3 Photo of rock sample

rockburst. Based on this process, we designed a corresponding time-delay rockburst test. Firstly, the rock sample is loaded into the stress state of five-sides loading and one face free. It simulates the real stress state of the surrounding rock during the actual excavation process. Then, the process of vertical stress concentration is restored by loading the maximum principal stress of the rock sample to a set value. Finally, the stress state of five-sides loading and one face free for the rock sample is maintained until the rockburst occurs. The schematic diagram of stress transformation of the rock element before and after excavation is shown in Fig. 4a (σ_v : Vertical principal stress; σ_H : Maximum horizontal principal stress; σ_h : Minimum horizontal principal stress).

The specific experimental scheme is described as follows. In order to prevent the rock sample from sliding towards the free face, the maximum principal stress σ_1 and the intermediate principal stress σ_2 are first loaded to the target value of σ_2 at a rate of 0.4 MPa/s. Then the load for σ_2 is maintained. The loading for σ_1 is continued at a rate of 0.4 MPa/s until it reaches to 100 MPa. Then, loading σ_3 to the its target value at a



(a) Schematic diagram of stress transformation of the rock element before and after excavation



(b) Stress loading path

Fig. 4 Schematic diagram of the test loading

rate of 0.4 MPa/s. Keep the magnitude of σ_2 and σ_3 unchanged, loading σ_1 separately until the AE hit rises rapidly. Maintain the stress state, after a period of time, the rock sample occurs rockburst. The stress loading path is shown in Fig. 4. Among them, the target values of σ_3 and σ_2 are 5 MPa and 30 MPa, respectively, which are empirical values (Su et al. 2016, 2017; Liu et al. 2023). According to the true triaxial test habits and related rock test procedures (Su et al. 2017; Zheng et al. 2023; Zhao et al. 2021), the loading rate is 0.4 MPa/s. The stress loading path is shown in Fig. 4b.

As shown in Fig. 4, in order to facilitate the subsequent analysis of this paper, the time-dependent failure effect of the rock sample in the load maintenance phase is called the time effect. The time elapsed between the


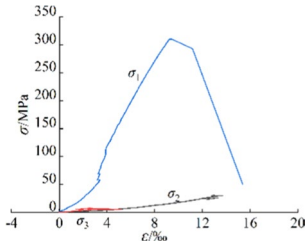

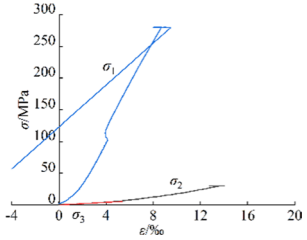

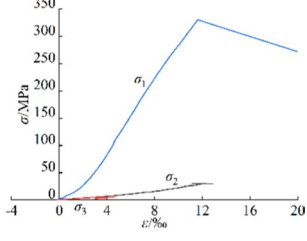
moment the loading stops, when the AE hits rises rapidly, and the time the rockburst occurs is defined as duration. The stage relates to the duration is defined as the time lag stage.

3 Macroscopic failure characteristics of time-delayed rockburst

3.1 Strength deformation characteristics

The typical experiment results of time-delayed rockburst are described in Table 1, which includes the failure phenomenon, host rock failure morphology, peak

Table 1 Test results of time-delayed rockburst

Sample number	Failure phenomenon of the free surface	Failure morphology of the host rock	Peak stress (MPa)	Stress–strain curve	Duration(s)
HG-1	When the vertical stress reaches 310 MPa, there was a crisp cracking sound. 6 s later, particle ejection appeared in the upper right corner of the free surface. 74 s later, a small block ejection appeared in the upper right corner. 17 s later, a large block ejection began to appear on the right side of the free surface, followed by a strong overall ejection failure of the rock sample, accompanied by a loud sound		310.061		99.72
HG-2	When the vertical stress reaches 278 MPa, local peeling and small particle ejection appeared in the upper right corner of the free surface, accompanied by a crisp cracking sound. 54 s later, a block ejection appeared in the upper right corner of the free surface. 30 s later, the upper part of the outer rock slab was broken, and the whole piece falls. 28 s later, the rock sample underwent strong ejection failure, accompanied by a loud noise		280.007		107.28
HG-3	When the vertical stress reaches 328 MPa, small particles ejection occurred in the upper right corner of the surface, accompanied by a crisp cracking sound. After 21 s, particle ejection appeared in the upper right corner of the free surface. 16 s later, a large number of particles were ejected continuously in the upper part of the free surface. 5 s later, the rock sample underwent strong ejection failure, accompanied by a loud noise		330.005		37.44

stress, stress–strain curve and duration of the rock sample. The experiment results showed that HG-2 sample has the longest duration, followed by HG-1 sample, and HG-3 sample has the shortest duration. In the table, when the maximum principal stress σ_1 is 100 MPa, the maximum principal strain ϵ_1 fluctuated due to the single-sided loading of the minimum principal stress σ_3 . When the rockburst occurs, the upper

surface of HG-2 sample tilted, resulting in a reverse growth trend of the maximum principal strain ϵ_1 .

The stress–strain curves of the rock samples are shown in Fig. 5. In loading stage, the maximum principal strain ϵ_1 increased with the increase of the maximum principal stress σ_1 ; during the lag phase, there was only a small increase for ϵ_1 (Fig. 5a). In the early stage of loading, the rock sample undergoes

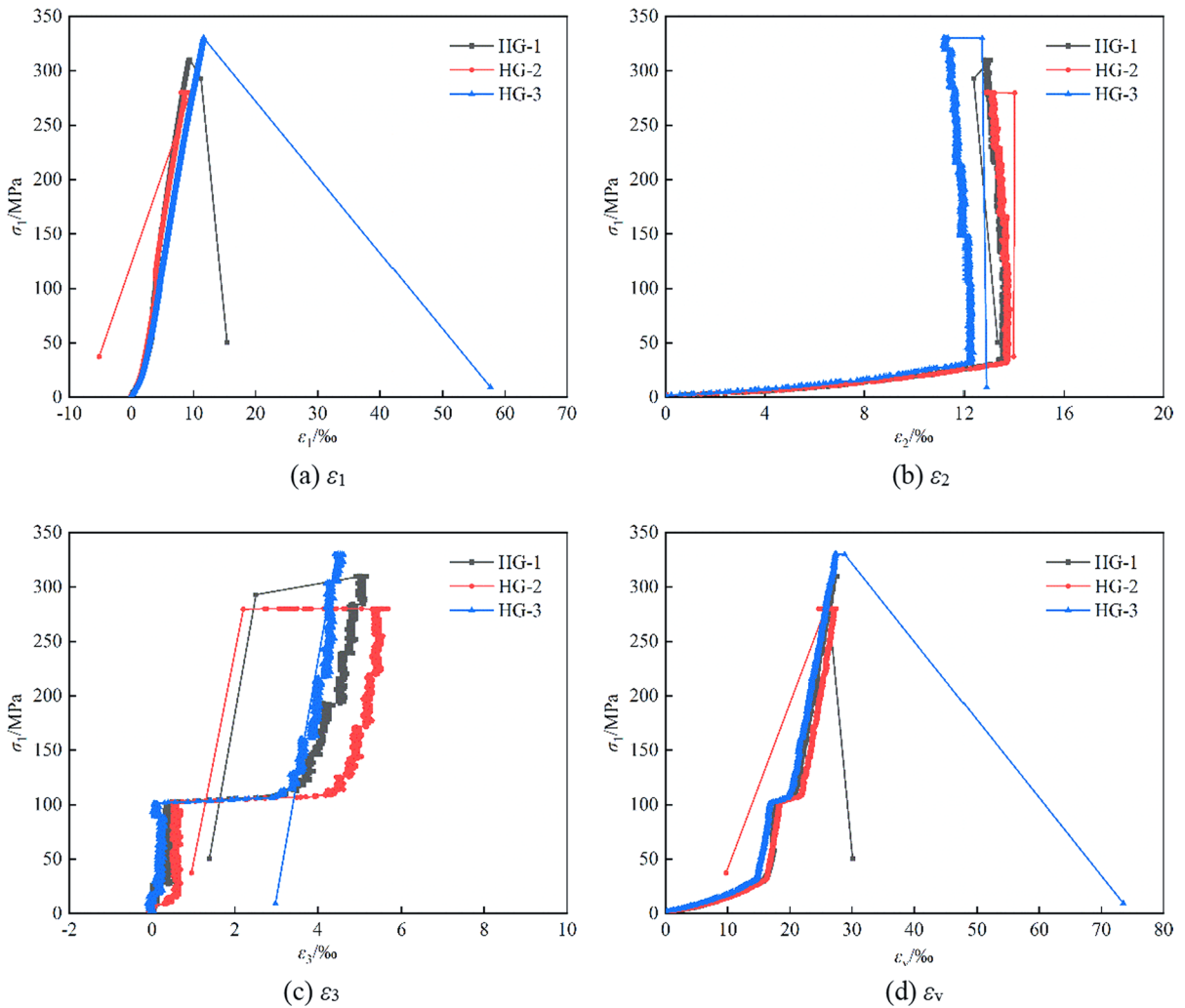


Fig. 5 Stress–strain curves of the rock samples

the compaction stage, and the intermediate principal strain ϵ_2 increased with the increase of the intermediate principal stress σ_2 . After σ_2 reaches the predetermined value of stop loading, ϵ_2 slowly decreased with the increase of σ_1 due to the Poisson effect. During the lag phase, ϵ_2 increased slowly (Fig. 5b). Due to the free face, the minimum principal strain ϵ_3 was greatly affected by the stress in the other two directions. In the early stage of loading, ϵ_3 slowly increased with the increase of σ_1 and σ_2 . After σ_2 reached the predetermined value of stop loading, σ_1 continues to load, however, without obvious change in ϵ_3 . When σ_1 increases to 100 MPa, the minimum principal stress σ_3 began to load, ϵ_3 increased rapidly

with the increase of σ_3 . After σ_3 reached the predetermined value of stop loading, ϵ_3 slowly increased with the increase of σ_1 . During the time lag phase, ϵ_3 slowly decreased (Fig. 5c). In the early stage of loading, the rock sample underwent the compaction stage, the strain in all three directions increased. The volume strain ϵ_v gradually increased, and the contraction trend of the rock sample was significant. After σ_2 reached the predetermined value and stopped loading, ϵ_3 is with no obvious change due to the slow decrease of ϵ_2 . Only ϵ_1 increases with the increase of σ_1 . Therefore, the contraction trend of the rock sample is significantly slowed down. When σ_1 increased to 100 MPa, ϵ_3 and ϵ_v increased rapidly. After σ_3

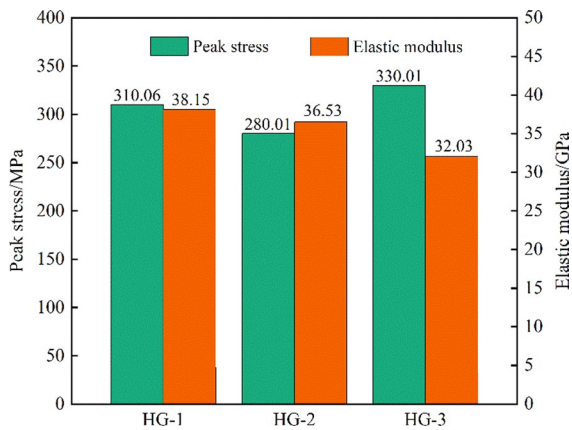


Fig. 6 Peak stress and elastic modulus of time-delayed rockburst test samples

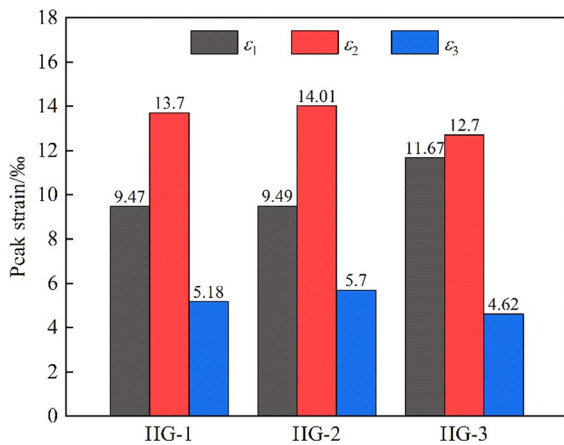


Fig. 7 σ_1 , σ_2 and σ_3 of the time-delayed rockburst test samples

reached the predetermined value and stops loading, ϵ_v slowly increased with the increase of σ_1 , during which a large amount of energy inputs to the rock sample. During the time lag phase, there was no significant change in ϵ_v (Fig. 5d).

According to the stress–strain curves in Table 1, the true triaxial peak stress σ_1 , the elastic modulus E_1 and the peak strain ϵ_1 in the direction of σ_1 of the granite sample can be obtained. The results are shown in Figs. 6 and 7. It can be seen that σ_1 of HG-1, HG-2 and HG-3 rock samples are 310.06, 280.01 and 330.01 MPa, respectively. The elastic modulus E_1 of HG-1, HG-2 and HG-3 rock samples are 38.15, 36.53 and 32.03 GPa, respectively. The peak strains

of HG-1, HG-2 and HG-3 are 9.47‰, 9.49‰ and 11.67‰ in the direction of σ_1 , 13.7‰, 14.04‰ and 12.7‰ in the direction of σ_2 and 5.18‰, 5.70‰ and 4.62‰ in the direction of σ_3 , respectively.

3.2 Ejection failure process analysis

The failure process of granite time-delayed rockburst is shown in Fig. 8. The failure process can be divided into four stages. (1) Grains ejection stage: after a period of calm, with the gradual increase of vertical loading, microcracks inside the rock sample begin to germinate and expand. A small number of grains and small blocks ejection appear many times in the upper right part of the free face, accompanied by cracking sound; (2) Slab break and eject stage: under the stress of constant load on five sides, there was visible crack propagation penetration at the ejection of the original grains, causing the free surface to crack and bulge. And then the surface rock of the free surface is with a local ejection phenomenon; (3) First fragments ejection stage: continuing to maintain the load, strong mixed ejection of pieces and grains began to appear at the cracking of the free surface, accompanied by a loud sound; (4) Second fragments ejection stage: continuing to maintain the five-sided constant load state, on the shallow V-shaped pit formed by the first fragments ejection, a violent second mixed ejection of blocks and grains occurred in the rock sample, and a deep V-shaped pit was formed, accompanied by a loud sound. The interval between the two fragment ejections is within 1–2 s. There are two fragments ejection in the failure process of the time-delayed rockburst, which is different from the ejection process in rockburst studied by Su et al. (2016).

The failure pattern of the host rock after the time-delayed rockburst is shown in Fig. 9. For the time-delayed rockburst sample, the macroscopic crack was with an obvious V-shaped shear crack composed of a penetrating shear crack far from the free face and a shear crack extending inward at the middle of the free face. Meanwhile, there were several tensile cracks in the lower part of the sample cross-penetrated with the “V” shear crack. The rock sample splits the rock plate due to tension, forming a large number of axial tensile cracks. Due to shear, multiple oblique shear cracks are formed on the inside of the rock.

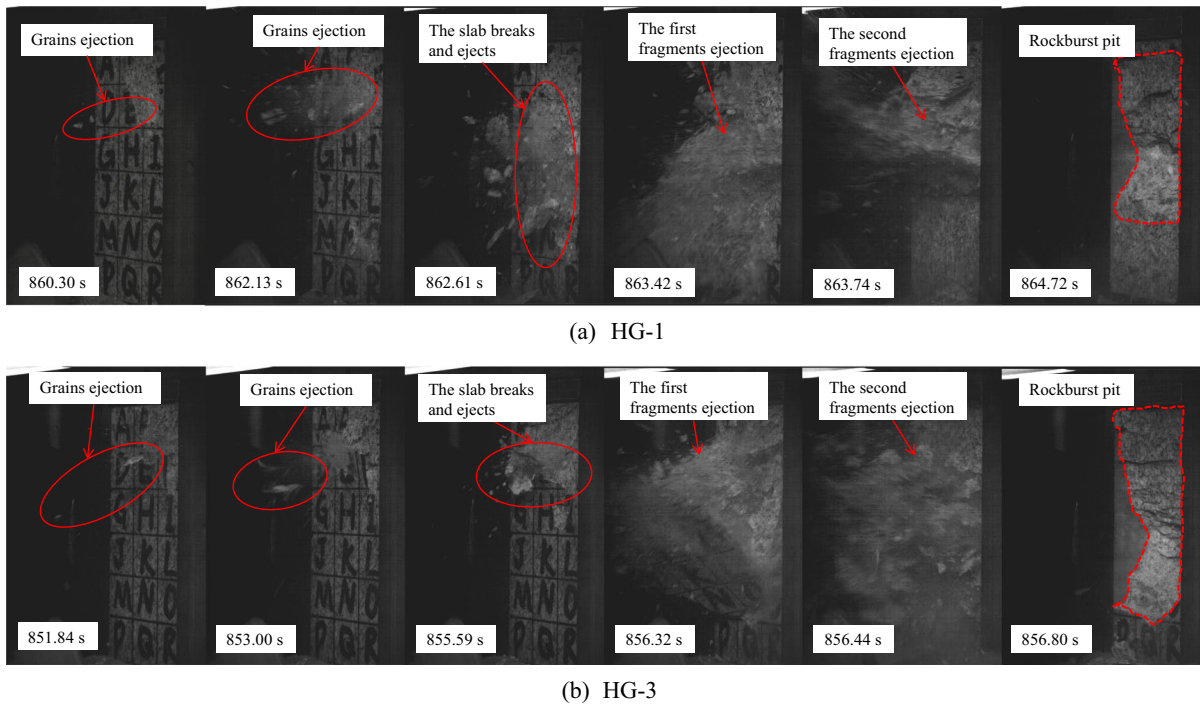


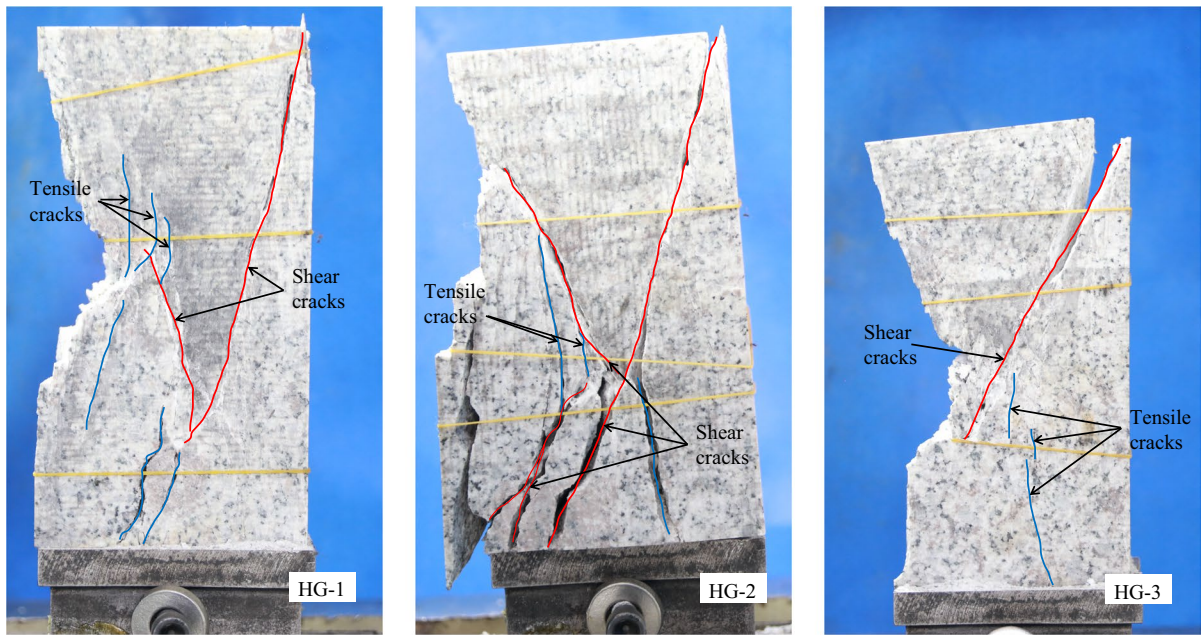
Fig. 8 Failure process of the time-delayed rockburst

It can be seen from Figure 9 that the tensile cracks at the bottom of the HG-2 rock sample were well developed, and the fractures formed by the crack penetration were dense and wide. The tensile cracks at the bottom of the HG-1 rock sample were dense, forming several tensile fractures. The tensile crack at the bottom of the HG-3 rock sample is not fully developed, and the tensile crack formed by the crack penetration cannot be directly seen. The longer the duration, the more fully developed the tensile cracks inside the rock sample. It shows that in the time lag stage after the rapid increase of AE hits, the tensile cracks at the bottom of the rock sample under the stress of five-sides constant load were fully developed. The longer the duration, the more obvious the splitting effect of the rock sample. And the tensile crack was developed fully. The tensile cracks formed was also denser. At the same time, the microcracks in the direction of the two main shear cracks fully developed and expanded. When the crack developed to a certain extent, the microcracks penetrate to form cracks, resulting in rockburst.

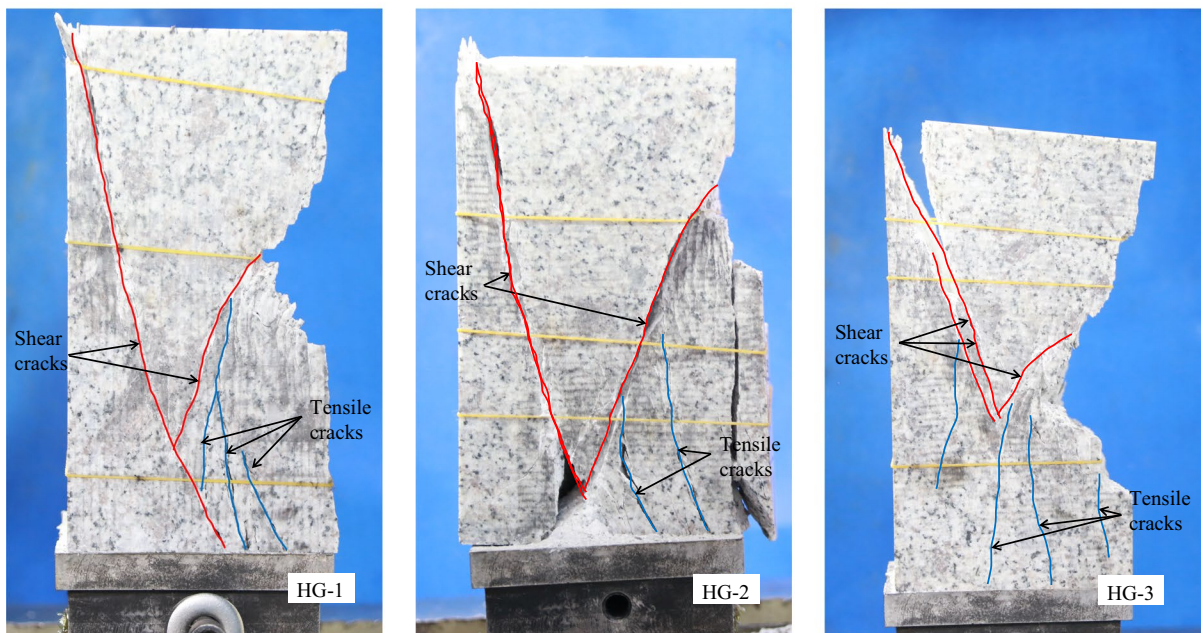
The maximum depth of the V-shape pit after the rockburst of HG-1, HG-2 and HG-3 rock samples

were 26.1 mm, 7.2 mm and 29.2 mm, respectively, from which it can be seen that the longer the duration of the rock sample, the smaller the depth of the rockburst pit. The maximum depth points of the V-shape pits in HG-1, HG-2, and HG-3 rock samples are 83.5 mm, 46.5 mm, and 110.7 mm from the upper surfaces of the samples, respectively, from which it can be seen that the longer the duration of the rock sample, the closer the maximum depth points to the upper surface of the rock sample.

According to the stress-strain curve, the total energy, elastic strain energy and dissipated energy before the rockburst of the rock sample can be calculated. And then the proportion of elastic strain energy and dissipative energy before the rockburst of each rock sample can be obtained (Ran et al. 2023; Wang et al. 2023; Xie et al. 2005). The proportions of elastic strain energy before rockburst in each rock sample was between 77.75 and 84.22%, and the proportions of dissipated energy was between 15.78 and 22.25%. The longer the duration, the smaller the proportion of elastic strain energy and the larger the proportion of dissipated energy. The longer the duration, the more fully developed the tensile cracks



(a) The left side of the rock sample is the free face



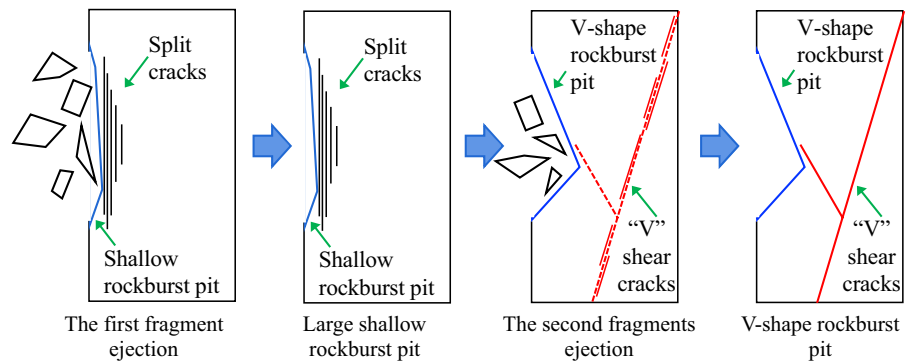
(b) The right side of the rock sample is the free face

Fig. 9 Fracture morphology of the rock samples

inside the rock sample. It will consume a lot of energy, which increased the proportion of dissipated energy and resulted in a decrease in the elastic strain energy used for the ejection of rockbursts in the rock

sample. The longer the duration, the more fully developed the cracks inside the rock sample. However, the related elastic strain energy was small and it can only cause rockburst ejection failure in the shallow part.

Fig. 10 Schematic diagram of the two ejections in the process of time-delayed rockburst



Therefore, the depth of the rockburst pit formed after the rockburst of the rock sample was small. It means that the longer the duration, the smaller the depth of the pit formed after the rockburst of the rock sample.

Combined with the failure pattern of rock samples, the mechanism of the two ejections in the process of time-delayed rockburst is analyzed, and it is shown in Fig. 10. Firstly, the rock sample was in a five-sides loading and one face free stress state. The surface of the free face was unevenly stressed and the area near it exhibits significant splitting under the maximum principal stress. Then it quickly split into plates and the first block ejection occurred in the surface of the free face, forming a large shallow rockburst pit (Light blue line in the figure).

The second ejection failure was due to the fact that the elastic strain energy stored inside the rock sample after the first fragment ejection was not fully released, and the newly generated free face has not reached a stable state. There are a large number of potential split cracks (Black line in the figure) near the free face, and a large number of the microcracks in the main shear direction were formed in the internal rock mass far away from the free face. Under the action of constant load on five sides, the microcracks in the main shear direction penetrates to form a "V" type shear crack (Red line in the figure). Under the action of maximum principal stress, the potential cracks near the free face connected and penetrated, and several small blocks formed in the surface rock. Under the action of the remaining elastic strain energy, the small blocks were rapidly ejected outward, and the second fragment ejection occurred. After the second fragment ejection, the rock sample failed and lost its strength instantly. It released a large amount of energy

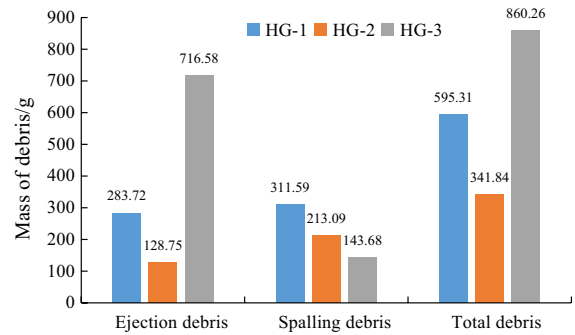


Fig. 11 Distribution of debris in each sample rock

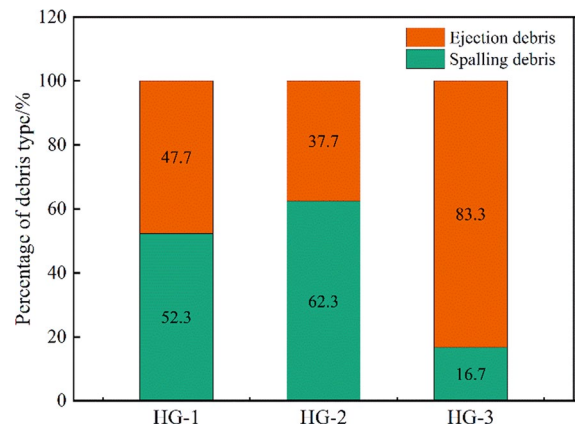


Fig. 12 Proportions of debris types of the rock samples

and formed a V-shape rockburst pit (Blue line in the figure).

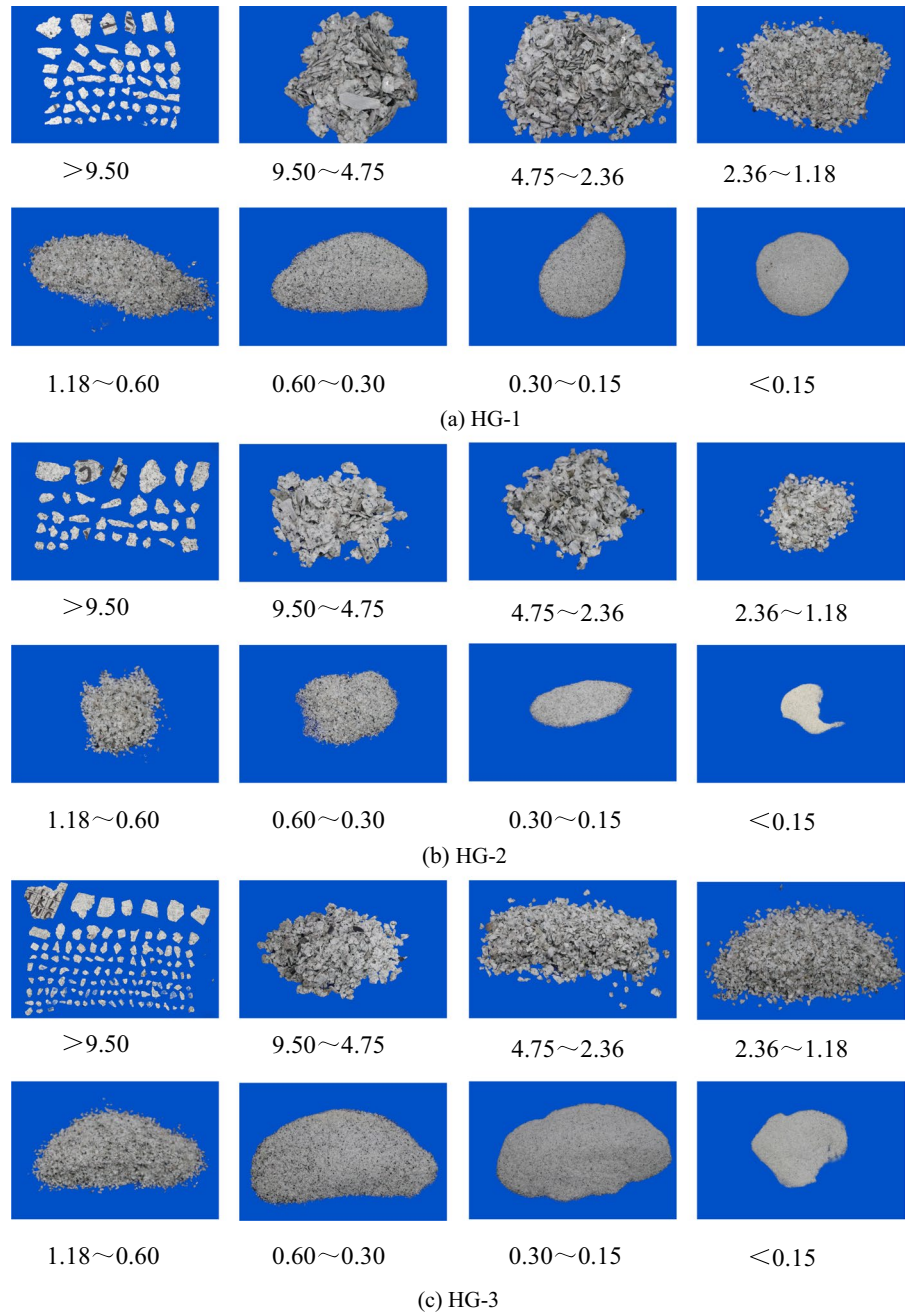
3.3 Debris characteristic analysis

Rockburst debris can reflect the occurrence mechanism of rock fragmentation process, which can be used as an effective mean to reveal the rockburst mechanism. According to the distance of the debris dropping, rockburst debris can be divided into ejection debris and spalling debris. All debris generated

during the test were collected and counted, and the results were shown in Fig. 11.

It can be seen from Fig. 11 that the HG-3 rock sample produced the most rockburst debris and its total rockburst debris mass was 860.26g. The total debris mass of the HG-2 rock sample was the smallest with a mass of 341.84g. And the total debris mass of HG-1 rock sample was 595.31g. It can be seen that

Fig. 13 Distribution of catapult debris in rock samples (mm). **a** HG-1, **b** HG-2, **c** HG-3



the duration is negatively correlated with the total debris mass, and the longer the duration, the smaller the total debris mass. Fig. 12 shows the type distribution of rock sample debris. It can be seen that the proportions of spalling debris were between 16.7 and 62.3%, and the proportions of ejection debris were between 37.7 and 83.3%. The longer the duration, the larger the proportion of spalling debris, and the smaller the proportion of ejection debris. The main reason for this is analyzed. In the time lag stage after the rapid rise of the AE hits, under the action of constant load of five-sides, the internal cracks of the rock sample were fully developed and penetrated. It consumed a lot of energy. The longer the duration, the more energy is consumed and the less energy is used for debris ejection at the time of rockbursting. It resulted in a decrease in the proportion of rock ejection debris and an increase in the proportion of spalling debris.

In order to study the distribution characteristics of true triaxial time-delayed rockburst ejection fragments, the ejection debris was treated by screening method. The screening sizes were >9.5 mm, 9.50–4.75 mm, 4.75–2.36 mm, 2.36–1.18 mm, 1.18–0.60 mm, 0.60–0.30 mm, 0.30–0.15 mm, and <0.15 mm, respectively. The distribution of fragments after screening for each rock sample is shown in Fig. 13.

The mass percentage of the debris of each screening grade can be obtained by weighing the ejection

debris of different screening grades and dividing it by the total mass of the ejection debris. The result is shown in Fig. 14. It can be seen from the figure that the mass percentage of debris with time-delayed rockburst ejection with debris size >9.50 mm was 50–70%. It indicates that the ejection debris is mainly fragments and pieces. For HG-3 rock sample with the shortest duration, the mass of ejected debris with the size >9.50 mm accounted for the largest, it is 69.97%. Combined with the macroscopic failure pattern of the time-delayed rockburst, it can be seen that rock sample with a short duration is with a large proportion of mass of large debris in ejected debris. The degree of ejection debris fragmentation was low, and the internal crack development was not sufficient. However, in long duration rock samples, the mass proportion of large debris in ejection debris was small, indicating that the ejection debris fragmentation degree was higher and the internal crack development was fully developed. It shows that in the time lag stage after the rapid increase of the AE hits, the longer the duration of the rock sample under the action of five-sides constant load, the fuller the internal crack development, accompanied by the formation of a large number of small fragments and grains.

The greater the mass and the faster the ejection velocity of ejected debris, the greater the kinetic energy of its ejection. Therefore, in the process of rockburst, the ejection kinetic energy of ejection debris can be used as an ideal index to quantitatively

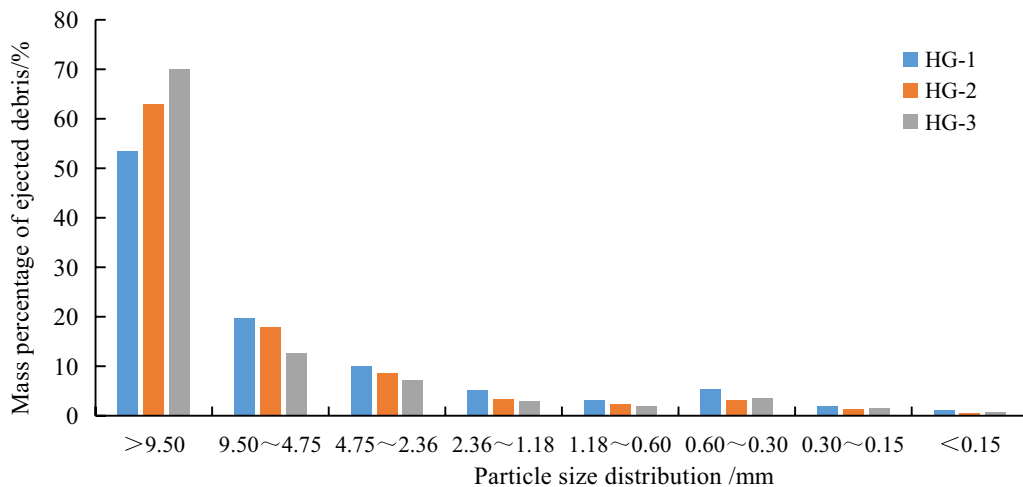


Fig. 14 Mass percentage of debris by sieving grade

Table 2 Ejection kinetic energy and mass of ejected debris for each rock sample

Sample number	Releasable elastic strain energy (J)	Ejection debris mass (g)	Kinetic energy (J)	Kinetic energy ratio (%)
HG-1	2435.18	283.72	2.11	0.09
HG-2	2092.86	128.75	1.03	0.05
HG-3	3286.50	716.58	3.56	0.11

evaluate the rockburst intensity, and the rockburst intensity can be reflected based on the ejection kinetic energy.

With the help of the high-speed camera system and professional image analysis software, the flight trajectory of the ejection fragments can be captured. Then, their ejection speed can be calculated based on the flight distance and time. After weighing their mass, the total kinetic energy of the ejection fragments can be calculated. The kinetic energy of ejection and the mass of ejection debris for each rock sample of time-delayed rockburst are shown in Table 2. It can be seen that the ejection kinetic energy of each rock sample accounted for 0.05–0.11% of the elastic strain energy that can be released before failure. And the longer the duration, the smaller the proportion. Within a certain range, the duration was roughly negatively correlated with the mass of ejection debris and ejection kinetic energy. The longer the duration, the smaller the ejection debris mass, the ejection kinetic energy of the rock sample, the rockburst intensity and the possible loss.

In the time-lag stage after the rapid increase of the AE hits, the microcracks inside the granite rock sample were fully developed and expanded under the action of five-sides constant load, consuming a lot of energy. The longer the duration, the more fully the microcracks inside the rock sample developed and expanded, and the more energy was consumed. Therefore, the ejection kinetic energy at the time of the rockburst was reduced. For time-delayed rockburst, the duration of rockburst evolution was crucial for the prevention and control of rockbursts. Within a certain range, its duration should be extended as much as possible, reducing its ejection debris mass and ejection kinetic energy, so as to reduce its possible losses.

Studies have shown that the particle size distribution of broken rock mass has fractal characteristics,

and fractal theory is widely used in the study of rock block fragmentation and particle size evolution. It can directly reflect the fracture and particle size distribution characteristics of broken rock before and after loading (Carpinteri et al. 2004). The fractal dimension value is a representation of the complexity of the composition of matter and its ability to self-organize, denoted by D .

According to the mass-frequency relation, the block distribution equation of the rock fragments can be obtained as follow.

$$M(d_i)/M_t = (d_i/d_{max})^{3-D} \quad (1)$$

where d_i is the particle size of the debris; $M(d_i)$ is the cumulative mass of the debris whose particle size is less than d_i ; M_t is the total mass of the debris; and d_{max} is the maximum size of the debris. Taking logarithm of both sides of Eq. (1), we can obtain that:

$$\lg[M(d_i)/M_t] = (3 - D) \lg(d_i/d_{max}) \quad (2)$$

According to Eq. (2), the slope of the fitted line in the $\lg[M(d_i)/M_t]-\lg(d_i/d_{max})$ coordinates is $3-D$, then the fractal dimension D can be obtained.

The fractal dimension fitting relation of the particle size distribution of each rock sample is shown in Fig. 15. The fractal dimension D values of HG-1, HG-2 and HG-3 rock samples are 2.0978, 2.1116 and 2.0902, respectively. It can be found that the fractal dimension increased with duration, which is roughly positively correlated with duration. The failure of the rock was caused by the initiation, development, expansion and penetration of a large number of internal tensile and shear cracks. In the time lag stage after the rapid rise of the AE hits, the granite rock sample under the action of five-sides constant load, the internal microcracks fully developed and expanded. It formed a large number of potential small fragments and small grains. The longer the duration, the larger the development and expansion of microcracks inside

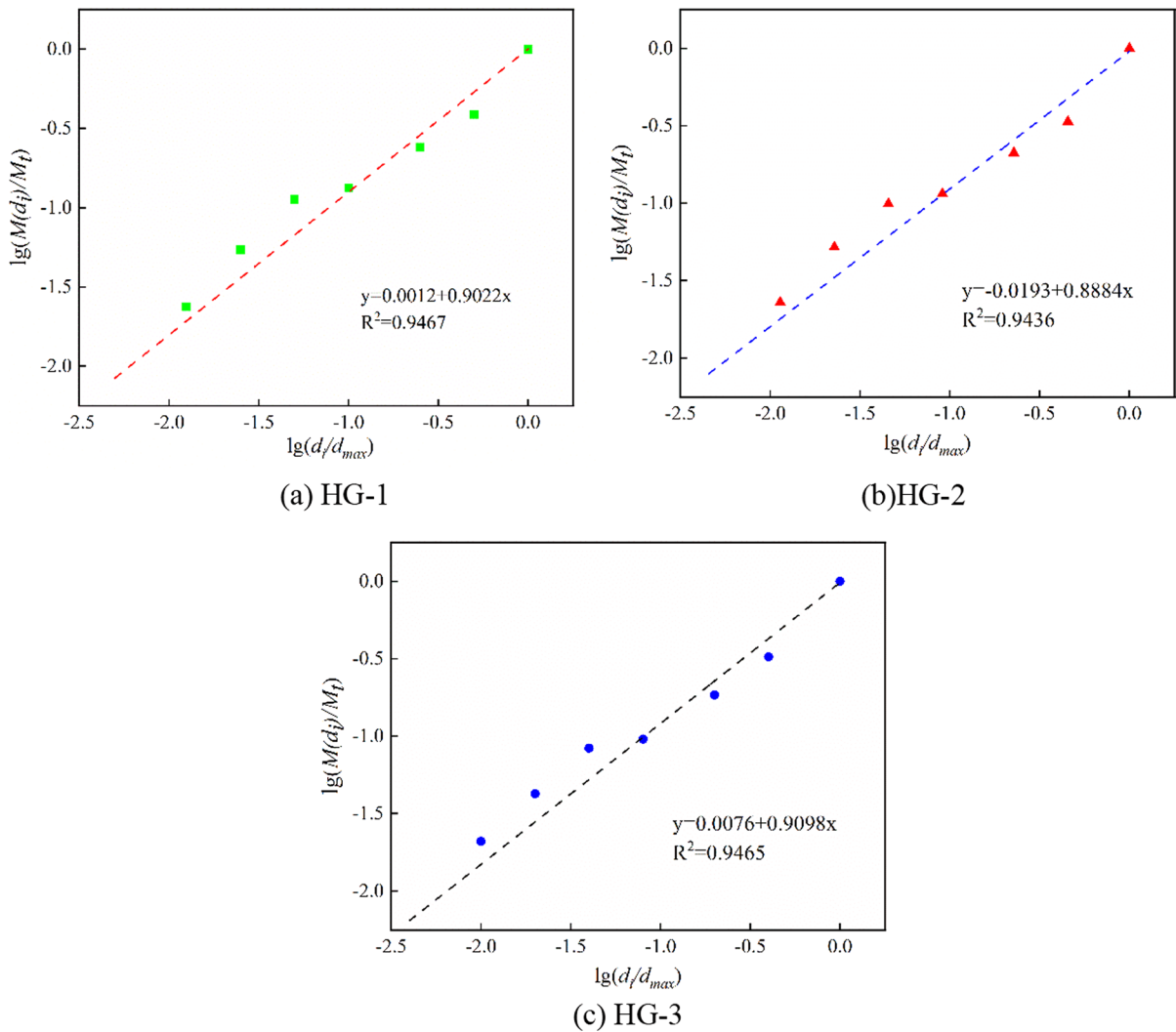


Fig. 15 Fractal dimension fitting relation of particle size distribution for each rock sample. **a** HG-1, **b** HG-2, **c** HG-3

the rock sample. Therefore, a lot of small fragments and small grains formed. In this way, the degree of fragmentation was very high, resulting in a large fractal dimension. By analyzing the detrital characteristics of rock samples, the relationship between the duration of time-delayed rockburst and the intensity of rockburst is revealed, the longer the duration, the smaller the ejection debris mass, the ejection kinetic energy of the rock sample and the rockburst intensity.

4 Internal crack evolution characteristics

4.1 RA and AF values

AE refers to elastic waves emitted by the development and expansion of internal fractures and the emergence of new cracks in rocks under force. The AE characteristics in rockburst development process can reflect the internal damage, fracture development and expansion of the rock. The AE waveform characteristics are generally considered to be an effective way to study the fracture failure mode (Chen et al. 2021; Su et al. 2020; Feng et al. 2023, 2023b).

Fig. 16 Schematic diagram of AE waveform parameters and crack classification

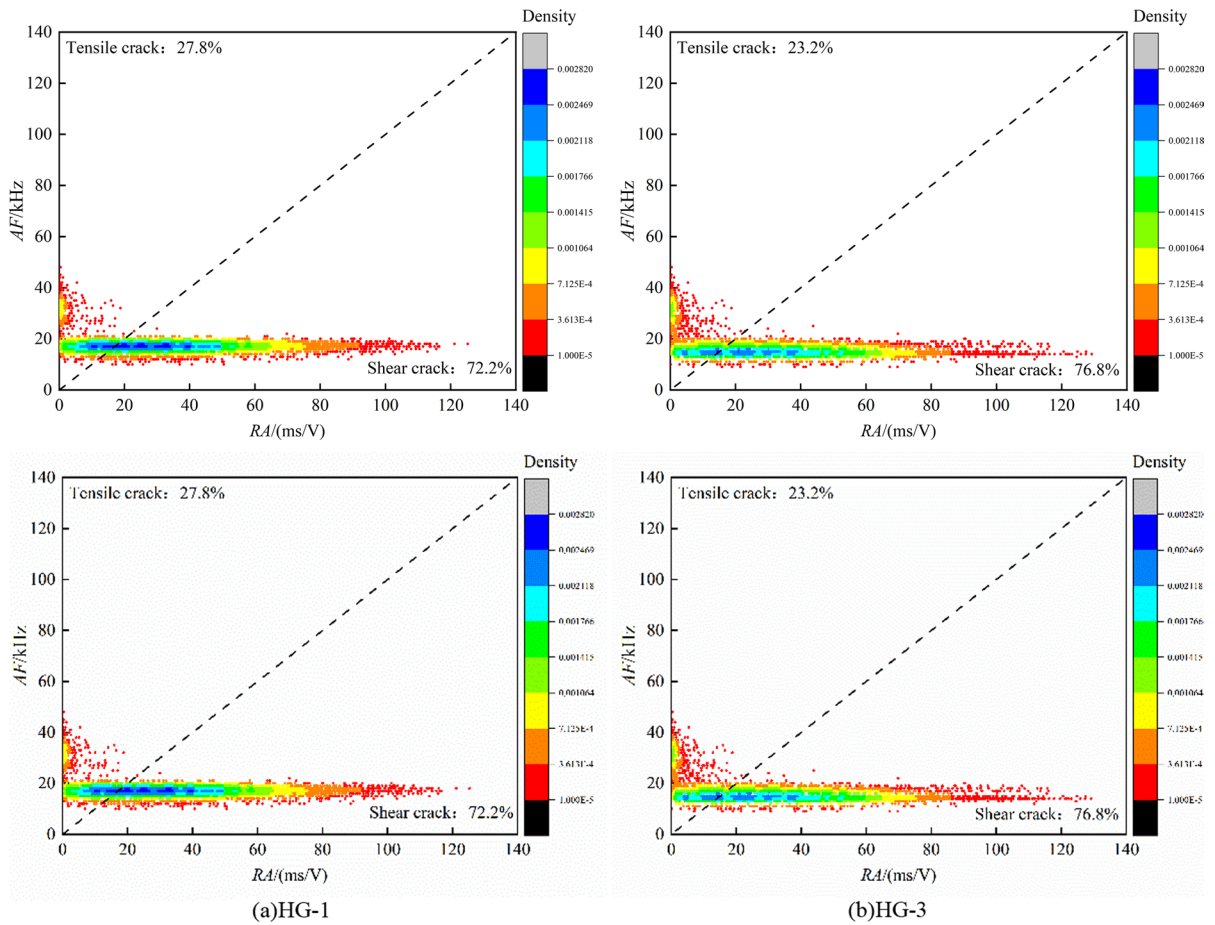
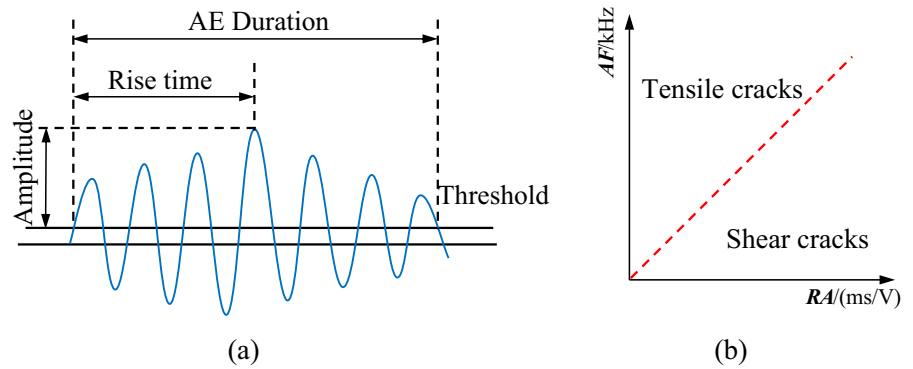


Fig. 17 RA-AF scatter distribution

Studies have shown that the RA value and AF (average frequency) value in the AE parameters can reflect the type of crack inside the rock (Carpinteri et al. 2016).

The RA value is the ratio of rise time and amplitude. The average frequency AF is the ratio of the count to AE duration. Generally, the AE signal with low AF and high RA value represents the emergence or development of shear cracks (He et al.

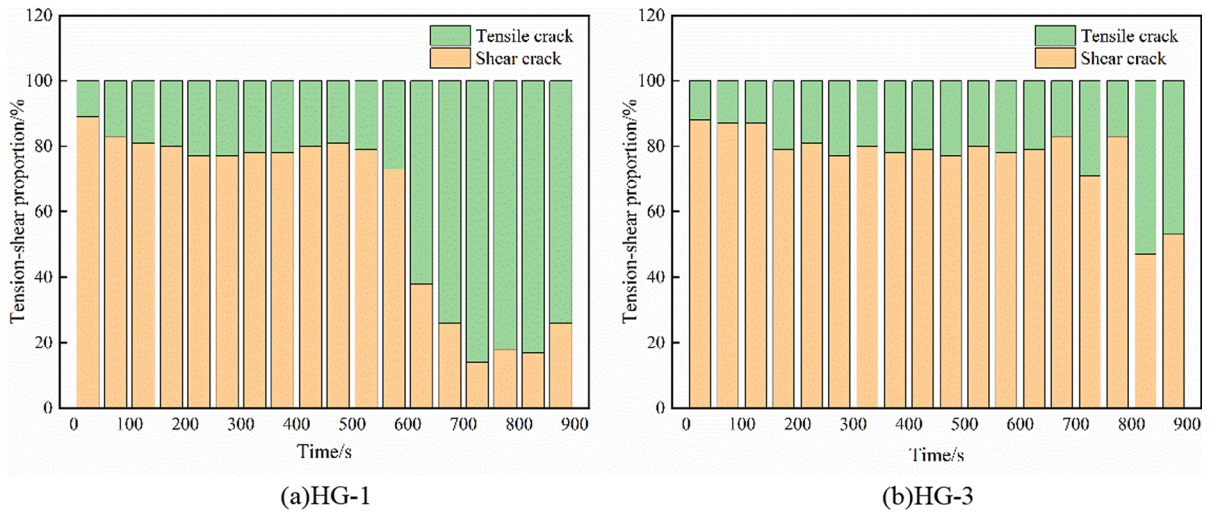


Fig. 18 Evolution of the tensile-shear proportion with time

2014). The high AF and low RA values indicate the emergence or development of tensile cracks. The schematic diagram of the basic parameters of AE waveforms and the classification of cracks are shown in Fig. 16.

The scatter density plots of RA and AF values in the time-delayed rockburst are shown in Fig. 17. It can be seen from the figure that the scatter distribution of the test data of each rock sample is generally the same, and the cracks produced by the rock sample are all tensile-shear composite cracks, in which the

shear cracks is the mainstay. The color of each point in the plot maps the smooth spatial density value at which that point is located.

Figure 18 shows the temporal evolution of the tensile-shear ratio in time-delayed rockburst for rock samples HG-1 and HG-3. It can be seen that the proportion of shear crack signal was 89.2%, and the proportion of tensile crack signal was 10.8% for HG-1 rock sample at the first 50 s. After 50 s, the proportion of shear crack gradually decreased, however, the shear crack was still dominated. The proportion

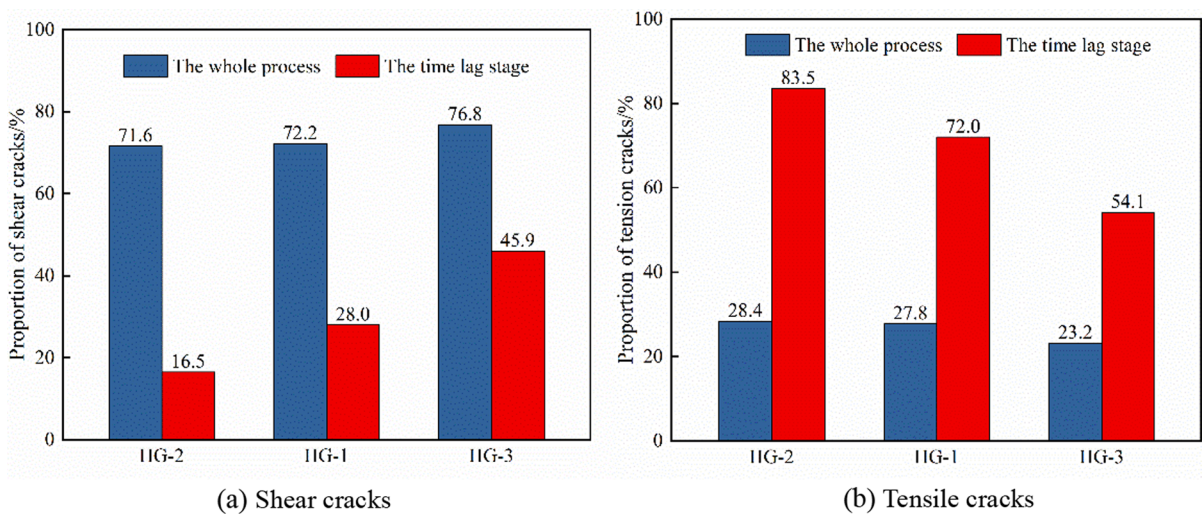


Fig. 19 Proportions of shear and tensile cracks in the whole process and time-lag stage of the time-delayed rockburst

of shear crack remained between 77.6 and 82.7%, and the proportion of tensile crack was between 17.3 and 22.4%. At 600–765 s, the proportion of shear crack dropped sharply to 14.1%, and the proportion of tensile cracks increased sharply to 85.9%. In the time lag stage after the rapid increase of the AE hits, the proportion of shear crack remained at ~20% and tensile cracks accounted for ~80% under the action of constant load on five sides. During the test of HG-3 rock sample at 0–150 s, the proportion of shear crack signal was 88.2%, and the proportion of tensile crack signal was 11.8%. After 150 s, the proportion of shear crack gradually decreased, however, the shear crack was still dominated. The proportion of shear crack remained between 70.9 and 82.8%, and the proportion of tensile crack was between 29.1 and 17.2%. At the moment of stopping loading after the rapid increase of the AE hits, the proportion of shear crack decreased sharply, accounting for ~43.9%, and the proportion of tensile crack increased sharply to 56.1%. In the subsequent time lag stage, the proportion of shear crack and tensile crack remained at ~45.9% and ~54.1% under the action of constant load on five sides. It can be found that the cracks produced in the development process of time-delayed rockburst rock are tensile-shear composite cracks, and the loading stage is mainly shear crack, and it is mainly tensile crack in the time lag stage.

Figure 19 shows the proportions of shear and tensile cracks in the whole process and time lag stage in the development process of the time-delayed rockburst. It can be seen that the proportion of shear crack in the whole process was in the range from 71.6 to 76.8%, and the proportion of tensile crack was 23.2–28.4%. The proportion of shear crack in the time lag stage of time-delayed rockbursts was in the range from 16.5 to 45.9%, and the proportion of tensile crack was 54.1–83.5%. The relation between the proportions of tensile crack and shear crack and the duration of each rock sample was analyzed. It was found that with the increase of the duration, the proportion of tensile crack increased and the proportion of shear crack decreased. It shows that in the time lag stage after the rapid increase of the AE hits, the longer the duration of granite rock sample under the action of constant load of five sides, the more likely the occurrence of tensile crack.

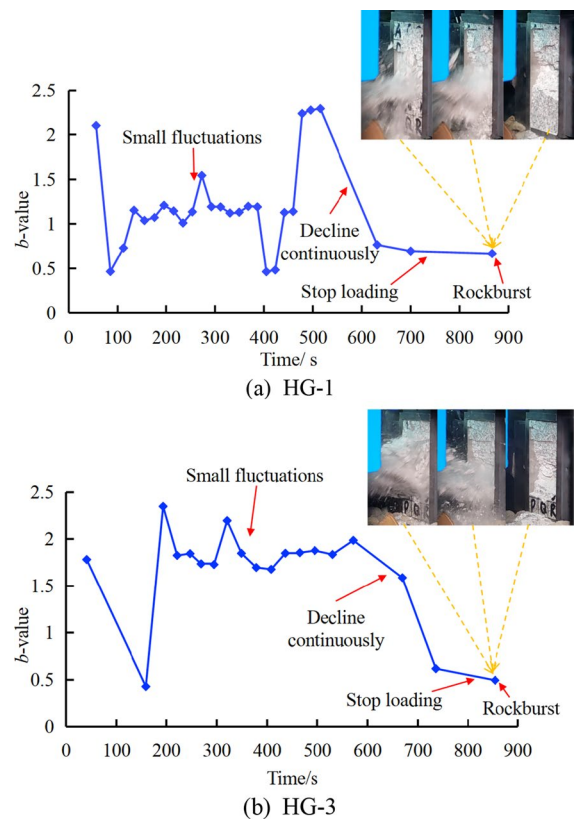


Fig. 20 Evolution law of b -value with time

4.2 b -value

The rock failure process can be analyzed by b -value, which is related to the magnitude and frequency of the earthquake. In 1941, Gutenberg et al. proposed the Gutenberg–Richter relation as follow (Gutenberg et al. 1944):

$$\lg N = a - bM \quad (3)$$

where M is the magnitude of the earthquake; N is the times of the earthquake magnitude exceeds or reaches M ; a , b are constants. In AE study, M is usually the amplitude divided by 20, i.e. $M=A/20$; A is the AE amplitude (dB); The b -value can characterize the scale of the magnitude distribution of AE events, and it is used to measure the relative number of small and large fracture events in the rock under compression condition. It is closely related to the development of rock fractures (Carpinteri et al. 2009).

To avoid the meaningless of b -value due to the low number of AE events within a certain magnitude range, 500 AE events were taken as a set of data for investigation. And 250 events are used as sliding windows to obtain the evolution law of b -value with the AE events. Combined with the correspondence between time and the AE events, the evolution law of the b -value with time was obtained. Taking the HG-1 and HG-3 samples as examples, the evolution of b -value with time during the time-delayed rockburst development process was analyzed, as shown in Fig. 20.

In the early stage at 1–133 s, the b -value of HG-1 rock sample fluctuated heavily. The maximum value was 2.1, and the minimum value was 0.5. After that, the b -value showed a slight fluctuation with time. It basically maintained at about 1.1. It means that the relative number of large events and small events was stable and the crack state of different scales (the distribution of fracture scales) was relatively constant. It represents a process of gradual stable expansion of fracture. In 386–477 s, the b -value fluctuated heavily. It falls to 0.5 at first and then rises to 2.2. The proportion of small-scale microcracks increased. In 477–495 s, the b -value continued to rise to the maximum value of 2.3. After that, the b -value decreased continuously, from the highest value of 2.3 to a low value of 0.7. The proportion of large-scale microcracks increased, indicating that the internal cracks of the rock sample showed an unstable expansion state. Microcracks penetrated to form cracks and rockbursts were about to occur.

In the early stage of test loading at 1–193 s, the b -value of HG-3 rock samples fluctuated heavily. It falls to 0.4 at first and then rises to 2.3. After that, the b -value showed a slight fluctuation with time. It basically maintained at about 1.8. The relative number of large events and small events was stable, and the crack state of different scales was relatively constant. It represents a gradual and stable expansion process. After 571 s, the b -value began to decrease continuously. It decreased from 2.0 to 0.5. It means that the proportion of large-scale microcracks increased. It indicates that the internal cracks of the rock sample was in an unstable propagation state, and the microcracks penetrated to form cracks. The rockburst was about to occur.

Therefore, the continuous decrease of b -value can be used as an effective prediction and early warning

information for the time-delayed rockburst. In addition, it can also be found that in the lag stage after the rapid increase of the AE hits, the b -value is at a low value. It indicates that the proportion of large cracks and small cracks inside the rock sample is relatively constant under the action of constant load on five sides at this stage. The b -value continuously decrease can be used as an effective prediction and early warning information for the time-delayed rockburst, which is consistent with the results of the immediate rockburst mainly studied by Su et al. (2020).

5 Conclusions

In this paper, the granite time-delayed rockburst test under true triaxial condition with AE and high-speed camera monitoring was designed and carried out. The failure characteristic and mechanism of granite time-delayed rockburst under true triaxial condition were studied. The main conclusions are as follows:

1. Under the true triaxial condition, the failure of granite time-delayed rockburst is with four stages, i.e. grains ejection, slab breaks and ejects, first fragments ejection and second fragments ejection. The elastic strain energy stored inside the rock sample was not fully released after the first ejection failure, and the newly generated free face did not reach a stable state. Under the action of constant load on five sides, the microcracks in the main shear direction penetrated to form a "V" shear crack, the potential cracks near the free face connected and penetrated and the surface rock formed several small blocks. Under the action of the remaining elastic strain energy, the small blocks were rapidly ejected outward, that is, the second fragments ejection occurred.
2. There is a "V" shear crack generated in the time-delayed rockburst sample. Several tensile cracks in the lower part of the rock sample crossed through the "V" shear crack. In the time-lag stage, the longer the duration, the more fully developed the cracks inside the rock sample. And a larger amount of energy was consumed, resulting in a decrease of the elastic strain energy for rock ejection. Therefore, it can only cause ejection failure in the shallow part of the sample, and the deep rock block cannot be ejected due to

insufficient kinetic energy of ejection. It means that the longer the duration, the smaller the depth of the rockburst pit.

3. The time-delayed rockburst debris were mainly composed of blocks and fragments. The longer the duration, the smaller the total debris mass, the percentage of ejected debris and the ejection kinetic energy. The fractal dimension of the debris was positively correlated with the duration. The longer the duration, the higher the degree of fragmentation. Therefore, for time-delayed rockburst risk mitigation, its duration should be extended as much as possible to reduce its ejection debris mass and ejection kinetic energy.
4. Under the true triaxial condition, the cracks generated in the development process of time-delayed rockburst are tensile-shear composite cracks. In the loading stage, it was dominated by shear cracks. However, in the time-lag stage, it was dominated by tensile cracks. With the increase of the duration, the proportion of tensile cracks increased and the proportion of shear cracks decreased.

Author contributions GF made substantial contributions to the design of the work and wrote the manuscript. QM carried out the experiments and data analysis and wrote the manuscript. GL revised the manuscript. PP and ZW supervised and writing—reviewed the manuscript. GS guided the test and revised the manuscript.

Funding The authors gratefully acknowledge financial support from the National Natural Science Foundation of China (grant no.41972295), the Guangxi Key Laboratory of Disaster Prevention and Engineering Safety, China (2019ZDK034) and the Project of Youth Innovation Promotion Association of Chinese Academy of Sciences (2021326).

Data availability The authors confirm they have included a data availability statement in their main manuscript file. The datasets generated during and/or analysed during the current study are available from the corresponding author on reasonable request.

Declarations

Ethics approval and consent to participate The authors declare that the submitted work is original and has not been submitted to more than one journal for simultaneous consideration.

Consent to publish The authors agree to publication in the Geomechanics and Geophysics for Geo-Energy and Geo-Resources and also to publication of the article in English by Springer in Springer’s corresponding English-language journal.

Competing interests The authors declare that they have no competing interests.

Open Access This article is licensed under a Creative Commons Attribution 4.0 International License, which permits use, sharing, adaptation, distribution and reproduction in any medium or format, as long as you give appropriate credit to the original author(s) and the source, provide a link to the Creative Commons licence, and indicate if changes were made. The images or other third party material in this article are included in the article’s Creative Commons licence, unless indicated otherwise in a credit line to the material. If material is not included in the article’s Creative Commons licence and your intended use is not permitted by statutory regulation or exceeds the permitted use, you will need to obtain permission directly from the copyright holder. To view a copy of this licence, visit <http://creativecommons.org/licenses/by/4.0/>.

References

- Bai JW, Li SC, Jiang YJ, Liu RT, Li ZF, Li W (2019) An extension theoretical model for grouting effect evaluation in sand stratum of metro construction. *KSCE J Civ Eng* 23(5):2349–2358
- Bai JW, Zhu ZJ, Liu RT, Wang M, Zhang QS, Ma H (2021) Groundwater runoff pattern and keyhole grouting method in deep mines. *Bull Eng Geol Env* 80:5743–5755
- Carpinteri A, Lacidogna G, Pugno N (2004) Scaling of energy dissipation in crushing and fragmentation: a fractal and statistical analysis based on particle size distribution. *Int J Fract* 129:131–139
- Carpinteri A, Lacidogna G, Puzzi S (2009) From criticality to final collapse: Evolution of the “*b*-value” from 1.5 to 1.0. *Chaos Solitons Fractals* 4:843–853
- Carpinteri A, Lacidogna G, Corrado M, Di Battista E (2016) Cracking and crackling in concrete-like materials: A dynamic energy balance. *Eng Fract Mech* 155:130–144
- Chen BR, Feng XT, Ming HJ, Zhou H, Zeng XH, Feng GL, Xiao YX (2012) Evolution law and mechanism of rockbursts in deep tunnel: time delayed rockburst. *Chin J Rock Mech Eng* 1:561–569 (in Chinese)
- Chen BR, Wei FB, Wang R, Li T, Zhu XH, Wang X (2020) Failure mechanisms and precursory characteristics of deep buried granite in a tunnel in Southwest China. *Chin J Rock Mech Eng* 39(3):469–479 (in Chinese)
- Chen HR, Di QY, Zhang WX, Li Y, Niu JR (2021) Effects of bedding orientation on the failure pattern and acoustic

- emission activity of shale under uniaxial compression. *Geomech Geophys Geo-Energ Geo-Resour* 7:20–37
- Fan Y, Lu WB, Wang YC, Yan P, Chen M (2015) Comparison of evolution characteristics of immediate and time delayed rockbursts under different excavation methods. *Chin J Rock Mech Eng* 34(Supp. 2):3715–3723 (in Chinese)
- Feng GL, Feng XT, Chen BR, Xiao YX, Yu Y (2015a) A microseismic method for dynamic warning of rockburst development processes in tunnels. *Rock Mech Rock Eng* 48(5):2061–2076
- Feng GL, Feng XT, Chen BR, Xiao YX (2015b) Microseismic sequences associated with rockbursts in the tunnels of the Jinping II hydropower station. *Int J Rock Mech Min Sci* 80:89–100
- Feng XT, Yu Y, Feng GL, Xiao YX, Chen BR, Jiang Q (2016) Fractal behaviour of the microseismic energy associated with immediate rockbursts in deep, hard rock tunnels. *Tunn Undergr Space Technol* 51:98–107
- Feng XT, Xiao YX, Feng GL, Yao ZB, Chen BR, Yang CX, Su GS (2019) Study on the development process of rockbursts. *Chin J Rock Mech Eng* 38(4):649–673 (in Chinese)
- Feng GL, Ma JG, Chen BR, Xiao YX, Jiang Q, Li PX, Lin MQ (2023a) Microseismic energy and intensity criterion of rockburst in deep TBM tunnels—A case study of the Neelum–Jhelum hydropower project. *J Central South Univ* 30:1695–1709
- Feng GL, Yoshida S, Lacidogna G (2023b) Special issue on new advances in acoustic emission and microseismic monitoring technologies in civil engineering. *Appl Sci* 13(2):969
- Guo HS, Sun QC, Feng GL, Li SJ, Xiao YX (2023) In-situ observations of damage-fracture evolution in surrounding rock upon unloading in 2400-m-deep tunnels. *Int J Min Sci Technol* 33:437–446
- Gutenberg B, Richter CF (1944) Frequency of earthquakes in California. *Bull Seismol Soc Am* 34(4):185–188
- He MC, Miao JL, Feng JL (2010) Rock burst process of limestone and its AE characteristics under true-triaxial unloading conditions. *Int J Rock Mech Min Sci* 47(2):286–298
- He MC, Nie W, Zhao ZY, Guo W (2012) Experimental investigation of bedding plane orientation on the rockburst behavior of sandstone. *Rock Mech Rock Eng* 45:311–326
- He MC, Zhao F, Du S, Zheng MJ (2014) Analysis of rock burst failure characteristics under different unloading rates. *Rock Soil Mech.* 35(10):2737–2747+2793 (in Chinese)
- Hedley DGF (1992) Rockburst handbook for Ontario hardrock mines. CANMET SP92-1E
- Jiang FF, Zhou H, Liu C, Sheng J (2019) Progress prediction and prevention of rockbursts in underground metal mines. *Chin J Rock Mech Eng* 38(5):956 (in Chinese)
- Kaiser PK, Tannant DD, McCreath DR (1996) Canadian rockburst support handbook. Geomechanics Research Centre/Laurentian University, Sudbury
- Liu XF, Feng XT, Zhou YY (2023) Influences of schistosity structure and differential stress on failure and strength behaviors of an anisotropic foliated rock under true triaxial compression. *Rock Mech Rock Eng* 56:1273–1287
- Ortlepp WD. RaSiM Comes of age—a review of the contribution to the understanding and control of mine rockburst. In: *Proceeding of the 6th International symposium on rockburst and seismicity in mines*. Nedlands: Australian Centre for Geomechanics. 2005; pp. 3–20
- Ran QC, Liang YP, Zou QL, Hong Y, Zhang BC, Liu H, Kong FJ (2023) Experimental investigation on mechanical characteristics of red sandstone under graded cyclic loading and its inspirations for stability of overlying strata. *Geomech Geophys Geo-Energ Geo-Resour* 9:11
- Rudajev V. High ground displacement velocities associated with rockburst damage. In: *Proceedings of the 3rd International symposium on rockburst and seismicity in mines*. Rotterdam: A.A. Balkema, 1993; pp. 101–106.
- Su GS, Jiang JQ, Feng XT, Mo C, Jiang Q (2016) Experimental study on the destruction process of rock blast ejection. *Chin J Rock Mech Eng* 35(10):1990–1999 (in Chinese)
- Su GS, Feng XT, Wang JH, Jiang JQ, Hu LH (2017) Experimental study of remotely triggered rockburst induced by a tunnel axial dynamic disturbance under true-triaxial conditions. *Rock Mech Rock Eng* 50(8):2207–2226
- Su GS, Gan W, Zhai SB, Zhao GF (2020) Acoustic emission precursors of static and dynamic instability for coarse-grained hard rock. *J Central South Univ* 27(10):2883–2898
- Wang RK, Xing WB, Yang YH (2016) Review on construction technologies of large-scale underground caverns in hydropower stations in China. *J Hydroelectr Eng* 35:1–11
- Wang CL, Du GY, Han Y, He K, Li EB (2023) Evolution characteristics of acoustic emission and strain energy for deep granite under different damage stages. *Geomech Geophys Geo-Energ Geo-Resour* 9(1):14–35
- Wu SC, Wu ZG, Zhang CX (2019) Rockburst prediction probability model based on case analysis. *Tunn Undergr Space Technol* 93:103069
- Xie HP, Ju Y, Li LY (2005) Rock strength and global failure criteria based on the principle of energy dissipation and release. *Chin J Rock Mech Eng* 24(17):3003–3010 (in Chinese)
- Zhang SC, Ma TH, Tang CA, Jia P, Wang YC (2020) Microseismic monitoring and experimental study on mechanism of delayed rockburst in deep-buried tunnels. *Rock Mech Rock Eng* 53:2771–2788
- Zhao HG, Song ZL, Zhang DM, Liu C, Yu BC (2021) True triaxial experimental study on mechanical characteristics and energy evolution of sandstone under various loading and unloading rates. *Geomech Geophys Geo-Energ Geo-Resour* 7(1):22
- Zheng Z, Zheng H, Zhao J, Liu ZB, Feng GL, Qiu SL (2023) Ductile–brittle quantitative evaluation of rock based on post-peak properties under true triaxial stress. *Geomech Geophys Geo-Energ Geo-Resour* 9:81

Publisher's Note Springer Nature remains neutral with regard to jurisdictional claims in published maps and institutional affiliations.